Title
A COMPARISON OF RESONANCE FORMATION IN n-p AND n+p REACTIONS

Author
Goldhaber, Sulamith.

Publication Date
1964-07-01

UCRL-11730

University of California

Ernest O. Lawrence Radiation Laboratory

A COMPARISON OF RESONANCE FORMATION IN π^-p AND π^+p REACTIONS

Berkeley, California

DISCLAIMER

Lecture at the Conference on Particle and High Energy Physics at Boulder, Colorado
June 29 - July 3, 1964

UCRL-11730

UNIVERSITY OF CALIFORNIA
Lawrence Radiation Laboratory
Berkeley, California

AEC Contract No. W-7405-eng-48

A COMPARISON OF RESONANCE FORMATION IN $\pi^- p$ AND $\pi^+ p$ REACTIONS

Sulamith Goldhaber

July 1964

Lecture at the Conference on Particle and High Energy Physics at Boulder, Colorado
June 29 – July 3, 1964

UCRL 11730
TG-93

A COMPARISON OF RESONANCE FORMATION IN $\pi^- p$ AND $\pi^+ p$ REACTIONS

Sulamith Goldhaber
Lawrence Radiation Laboratory
University of California
Berkeley, California

I. INTRODUCTION

For an experimentalist to penetrate the sanctum of the study of detailed dynamics of interactions is a dangerous occupation. There is the natural tendency to oversimplify and separate processes on the basis of their dominance over others. This "first order approximation" has been applied to the interpretation of our data. In this experiment we analyzed two seemingly simple reactions:

$$\pi^+ + p \rightarrow \pi^+ + \pi^- + p + \pi^+ \qquad (1)$$

$$\pi^- + p \rightarrow \pi^- + \pi^+ + p + \pi^- \qquad (2)$$

Both reactions have four strongly interacting particles which we found to interact in pairs and in triplets to form resonances. In order to investigate these resonances we have chosen to examine these two-and three-particle systems when produced in peripheral collisions. The obvious advantage to this method is the predominance of single particle exchange in peripheral collisions. The large scattering cross sections between the incident particle and the exchanged one in a given angular momentum state, leads to an enhancement in resonance production. Fig. 1 shows various possible Feynman diagrams for single particle exchange type peripheral collisions leading to resonances observed in this experiment. I will leave the analysis of the A^- production out of my discussion since it has been treated by Gerson Goldhaber's summary on this subject.[1]

Comparing reactions (1) and (2) there are a number of differences I would like to list:

(a) The isotopic spin of the initial state of reaction (1) is a pure $T = 3/2$ state whereas the one of reaction (2) is a mixed $T = 1/2$ and $T = 3/2$ state.

(b) In reaction (1) we anticipate a strong double resonance formation, i.e., $\rho^{o} + N^{*++}(1238)$ whereas in reaction (2) the double resonance formation has the neutral isobar $N^{*o} \rightarrow p\pi^{-}$ whose intensity is ~10% of the doubly charged one.

(c) Reaction (2) has a strong single resonance channel competing with the doubly resonating one, i.e., $N^{*++}(1238) + \pi^{-} + \pi^{-}$ whereas in reaction (1) the analogous channel corresponds to the one involving the lower intensity $N^{*o}(1238)$ isobar, i.e., $N^{*o}\pi^{+}\pi^{+}$.

Now let us see what the experiment shows.

II. THE TWO-PARTICLE RESONANCES

The double resonance formation in reaction (1) is illustrated in the triangle plot in Fig. 2. The large concentration of the events at the crossing of the bands is the proof of the strong enhancement in the double resonance channel. The data for the $p\pi^{-}$ interaction are shown in Fig. 3. Here we show the two-particle mass combinations for $\pi^{+}\pi^{-}$, $p\pi^{+}$, and $p\pi^{-}$. Since two negative pions are present in the channel we show two pairs for each event. We see here that a strong ρ^{o} meson formation as well as strong N^{*++} formation occurs. Although the presence of the neutral isobar can be noted, it stands out more clearly when produced together with the ρ meson. In Fig. 4 we show the $p\pi^{-}$ mass distribution for events in which a ρ^{o} meson is also present. Here we not only see the 3/2 3/2 neutral isobar but also the $T = 1/2$ $N^{*o}(1510)$

and $N^{*o}(1688)$ isobars. The observed energies, E, and respective full width at half maximum, Γ, are given in Table I.

TABLE I

Observed E and Γ Values for the Channels:

$$\pi^- p \rightarrow N^{*o} + \pi^+ + \pi^- \quad \text{and} \quad N^{*o} \rightarrow \pi^- p$$

Isobar	$E_{Observed}$(MeV)	Γ(MeV)
$N^{*o}_{3/2}(1238)$	1220	120
$N^{*o}_{1/2}(1510)$	1480	120
$N^{*o}_{1/2}(1688)$	1690	100

III. THE ASYMMETRY IN $\pi\pi$ SCATTERING

The double resonance channel in both reaction (1) and reaction (2) provides an excellent opportunity to investigate the single pion exchange mechanism. As Gerson pointed out in his talk we have observed a nice example of single pion exchange in the reaction $K^+ + p \rightarrow K^{*o} + N^{*++}$. It seemed to us that the $\rho + N^{*++}$ channel affords a similar opportunity to look at single pion exchange. We thus selected all double resonance events and then focused our attention on those with small four-momentum transfer. For $\pi\pi$ scattering leading to a 1^- state one expects the scattering amplitude to be of the form $P_1^o = \cos\alpha$, i.e., $\cos^2\alpha$ for the angular distribution. Here α is the angle between the scattered and incident pion in the ρ center of mass system.

In interactions leading to three particles in the final state, i.e., $\pi^- + p \rightarrow n\pi^+\pi^-$, asymmetries in the $\pi\pi$ scattering angle for ρ^o formation have been observed and attributed to either interference with non-resonating s- and

p-waves or to a singlet s-wave resonance.[2] The latter interpretation was offered to explain the fact that the asymmetry parameter (F-B)/(F+B) remained positive throughout the $\pi\pi$ effective mass region from threshold through the ρ resonance and beyond. We have also observed such asymmetries in the double resonance formation, $\rho^o + N^*(1238)$, both in the $\pi^+ + p$ and in the $\pi^- + p$ interactions. The first sample we investigated included events with four-momentum transfer, up to $\Delta^2_{\pi\pi} < 20\ m^2_\pi$. To select predominantly the p-wave $\pi\pi$ amplitude we reduced the sample to include $\Delta^2_{\pi\pi} < 5\ m^2_\pi$ only. The asymmetry which we expected to decrease remained at about the same level. The question arose now, whether the one pion exchange model is in jeopardy in this reaction or whether other reactions, such as represented by diagram (d) in Fig. 1 are playing an important role. To test the single 0^- exchange model we examined both the Treiman-Yang angle* and the correlation between the $\pi\pi$ scattering angle in the ρ^o center of mass the the $p\pi$ scattering angle in the N^* center of mass. In Fig. 5a we show such a correlation plot. It is obvious that the two scattering angles are <u>not</u> independent of each other. To demonstrate this point further we selected events in the two polar and equatorial regions of the $\pi\pi$ scattering angular distribution and examined for those events the $p\pi$ scattering angles (see Figs. 5e, 5f, and 5g). We would expect for single 0^- exchange the $p\pi$ scattering to be completely independent of the $\pi\pi$ scattering angle. We see, however, pronounced differences in the $\cos\alpha_N^*$ distributions. A similar but not as striking effect is seen in the $\pi\pi$ scattering angular distribution for events selected for the polar and equatorial region of the $p\pi$ scattering angle (see Fig. 5b, 5c, and 5d). The observed correlations led us to examine a possible three-particle state such as $(p\pi^+\pi^-)$ which could cause both the observed asymmetry as well as the correlations.

---

* For details see Reference 1.

I will now mainly confine myself to the results of such an investigation in the $p\pi^-$ system. In Fig. 6 we show the observed (π, π) scattering angle associated with the ρ^o(see Figl 1a). As mentioned in my introductory remarks a competing $N^{*++}\pi^-\pi^-$ channel is present in this reaction. The importance of this competing channel is demonstrated in Fig. 7 in which we show a scatter plot of the invariant masses of $p\pi^+$ versus $\pi^+\pi^-$. A large overlap region between the two resonance bands is noted. This overlap has a crucial effect on the $\pi\pi$ scattering angle. In Fig. 6 the shaded area gives the distribution of events after the $N^{*++}(1238)$ isobar has been removed. It is clear from examining this figure that the major part of the asymmetry comes from the overlap of the two resonances. We therefore feel that in the present data neither interference with s-and d-waves nor the existence of a scalar meson need be invoked to explain the asymmetry.

The next question we would like to pose concerns the N^{*++} isobar. If directly produced in the primary collision it would be formed together with a pair of negative pions (see Fig. 1b). For the events produced with small momentum transfer to the $(p\pi^+)$ system, we expect the single pion exchange to dominate. We have made two tests to check for single pion exchange: (a) the πp scattering angle in $(p\pi^+)$ center of mass which should follow a $1 + 3\cos^2\alpha$ distribution, and (b) the Treiman-Yang angle which is expected to be isotropic. Figs. 8 and 10 show the two distributions. The distribution in the scattering angle shows considerable interference effects while the Treiman-Yang angle is consistent with being isotropic. To examine interference effects with the ρ meson we looked at the distribution including and excluding events (see shaded area in Figs. 8 and 10) in the $N^{*++}-\rho$ overlap region. The evidence for an aligned N^{*++} isobar is thus inconclusive. For comparison we show in Fig. 9 the decay angular distribution for the events with N^{*o} isobar formation. The data here are consistent with $1 + 3\cos^2\alpha$.

IV. THE THREE-PARTICLE SYSTEM $p\pi^+\pi^-$

One further diagram which may possibly contribute to the reaction under discussion is given in Fig. 1d. To study this channel we looked at a Dalitz plot corresponding to the following three "particles" $N^{*o}(1238)$, π^+ and π^-. In Fig. 11, we show such a diagram in which we plot the square of the $(N^{*o}\pi^+)$ mass on the x-axis and that of the $(\pi^+\pi^-)$ mass on the y-axis. A clear band corresponding to a mass of 1400-1640 MeV is seen crossing the ρ^o band. A projection of the $M^2(N^{*o}\pi^+)$ axis shows a marked peak at a mass value $M(p\pi^+\pi^-)$ = 1520 MeV and Γ = 240 MeV. The shaded area shows the events outside the ρ^o band. If we now investigate the structure of the three-particle mass peak we find that the proton forming the N^{*o} forms a $p\pi^+$ mass which lies in the $N^{*++}(1238)$ mass region (see Fig. 13). In Fig. 12 we show a Chew-Low plot of the $N^{*o}\pi^+$ events. A strong clustering of events at low four-momentum transfer to the three-particle system is evident, indicating peripheral production of the mass peak. Here we must note that at the lower vertex in Fig. 1d we can form a nucleon isobar in T = 1/2. 3/2. and 5/2 states. While the observed peak is centered at the location of the $N^*_{1/2}(1510)$ it is considerably broader than the accepted value for that isobar.[3] We suspect that other states such as the shoulder in the T = 3/2 state may also contribute to the peak. The asymmetry in the ρ^o can now be understood to arise in part from the overlap of the ρ^o with the three-particle state which in turn decays to the N^{*++} isobar. We must further note that another possible origin for the observed mass peak may be interference effects between diagrams 1a and 1b taking into account the Bose symmetrization of the two negative pions.[4]

V. THE CHANNEL $N^{*++} + \pi^- + \pi^-$

Finally, we would like to discuss the properties of the two identical bosons, $\pi^-\pi^-$. The most surprising feature is the distribution in the $\pi^-\pi^-$ scattering angle (see Fig. 14). The distribution has all the earmarks of an

aligned high angular momentum state. We cannot find, however, any particular mass enhancement associated with the angular distribution. In a study of a correlation between the $N^{*0}\pi^+$ mass and the $\pi^-\pi^-$ scattering angle we find that the above mentioned three-particle mass peak is directly related to the anisotropy in the $\pi^-\pi^-$ scattering angle. The anisotropy may thus be due in part to the observed mass peak, although the presence of T = 2 d-wave scattering in the $\pi^-\pi^-$ system cannot be ruled out. The symmetry in the distribution shown arises from the fact that the two negative pions are indistinguishable.

To summarize the π^-p interaction we list all the channels feeding the four-particle final state in Table II. The data discussed here come from an experiment carried out in a momentum analyzed negative π beam of the Lawrence Radiation Laboratory's Bevatron using the 72-inch hydrogen bubble chamber as detector. The kinematic fitting and ionization information reduces the number of events with ambiguous interpretation to less than 1%. The measurements of all events produced in the π^-p interaction have been carried out with the "Flying Spot Digitizer"(FSD) of the Lawrence Radiation Laboratory. The people who have participated in various phases of this work are: John L. Brown, Gerson Goldhaber, John A. Kadyk, Benjamin C. Shen, George H. Trilling, and myself.

REFERENCES

1. Talk by Gerson Goldhaber at this conference.

2. G. Puppi, Annual Review of Nuclear Science, Vol. 13, p. 287 (Annual Reviews, Inc., Palo Alto, California 1963), Editor, E. Segre. Saclay-Orsay-Bari-Bologna Collaboration, Nuovo Cimento 29, 515 (1962). V. Hagopian and W. Selove, Proceedings of the Athens Conference on Recently Discovered Particles, p. 270, Ohio University Press, Athens, Ohio, 1963.

3. P. Bareyre, C. Bricman, G. Valladas, G. Villet, J. Blizard, J. Seguinot, Phys. Letters 8, 137 (1964). Extensive compilation of total cross sections and inelastic cross sections up to 700 MeV. J. A. Helland, C. D. Wood, T. J. Devlin, D. E. Hagge, M. J. Longe, B. J. Moyer, and V. Perez-Mendez, "Elastic Scattering of Negative Pions on Protons in the Energy Range 500 to 1000 MeV", Phys. Rev. (to be published).

4. We have greatly benefited from discussions with Professor F. Low on this subject.

FIGURE CAPTIONS

Fig. 1 Feynman diagrams for reactions

(a) $\pi^- + p \rightarrow \rho^o + N^{*o}$

(b) $\pi^- + p \rightarrow \pi^- + \pi^- + N^{*++}$

(c) $\pi^- + p \rightarrow A^- + p$

(d) $\pi^- + p \rightarrow \pi^- + N^{*o}\pi^+$

Fig. 2 Triangle plot for the reaction $\pi^+ + p \rightarrow (\pi^+ + \pi^-) + (\pi^+ + p)$

Fig. 3 Mass distributions of the two-particle $(\pi^-\pi^+)$, $(p\pi^+)$, and $(p\pi^-)$ states.

Fig. 4 Mass distributions of $(p\pi^-)$ state formed in the reaction $\pi^- + p \rightarrow \rho^o + p + \pi^-$

Fig. 5. Correlation plot between $\cos\alpha_\rho$ and $\cos\alpha_N^*$ for the $\pi^+ + p$ reaction

Fig. 6 Distribution in π^-, π^- scattering angle in ρ^o center of mass

Fig. 7 Scatter diagram of $(\pi^+\pi^-)$ mass versus $(p\pi^+)$ mass

Fig. 8 Distribution in p, π^+ scattering angle in $p\pi^+$ center of mass

Fig. 9 Distribution in p, π^- scattering angle in $p\pi^-$ center of mass

Fig. 10 Treiman-Yang angle computed at N^{*++} vertex

Fig. 11 Dalitz plot of $M^2(N^{*o}\pi^+)$ versus $M^2(\pi^+\pi^-)$ with respective projections

Fig. 12 Chew-Low plot of $M^2(N^{*o}\pi^+)$

Fig. 13 Invariant mass distribution of $p\pi^+$ for events in mass peak $1400 < M(N^{*o}\pi^+) < 1640$ MeV

Fig. 14 Distribution in π^-_{in} π^-_{out} scattering angle in π_1^-, π_2^- center of mass

Table II. Cross sections for the various channels in the reaction

$$\pi^- + p \longrightarrow \pi^+ + \pi^- + p + \pi^-$$

Channel	Events		Cross Section[(a)] mb	
1. $\rho^o + \begin{matrix} N^{*o}(1238) \\ N^{*o}(1510) \\ N^{*o}(1688) \end{matrix}$	50 44 46	140	0.085 ± .025 0.075 ± .025 0.078 ± .025	0.24 ± .07
2. $\rho^o\pi^-p \begin{matrix} \nearrow A^-p \\ \searrow \rho^o\pi^-p \end{matrix}$	160[(b)] 130	290	0.27 ± .08[(b)] 0.23 ± .07	0.50 ± .15
3. $N^{*++}\pi^-\pi^- \begin{matrix} \nearrow (p\pi^+\pi^-)\pi^- \\ \searrow N^{*++}\pi^-\pi^- \end{matrix}$	90 170	260	0.15 ± .05 0.29 ± .10	0.44 ± .11
4. $\begin{matrix} N^{*o}(1238)\pi^+\pi^- \\ \pi^+\pi^-p\pi^- \end{matrix}$	340		0.60 ± .2	
TOTAL	1030		1.8 ± 0.4	

(a) all cross sections have been normalized to the total π^-p cross section.

(b) the events in the A_1 and A_2 regions are included here.

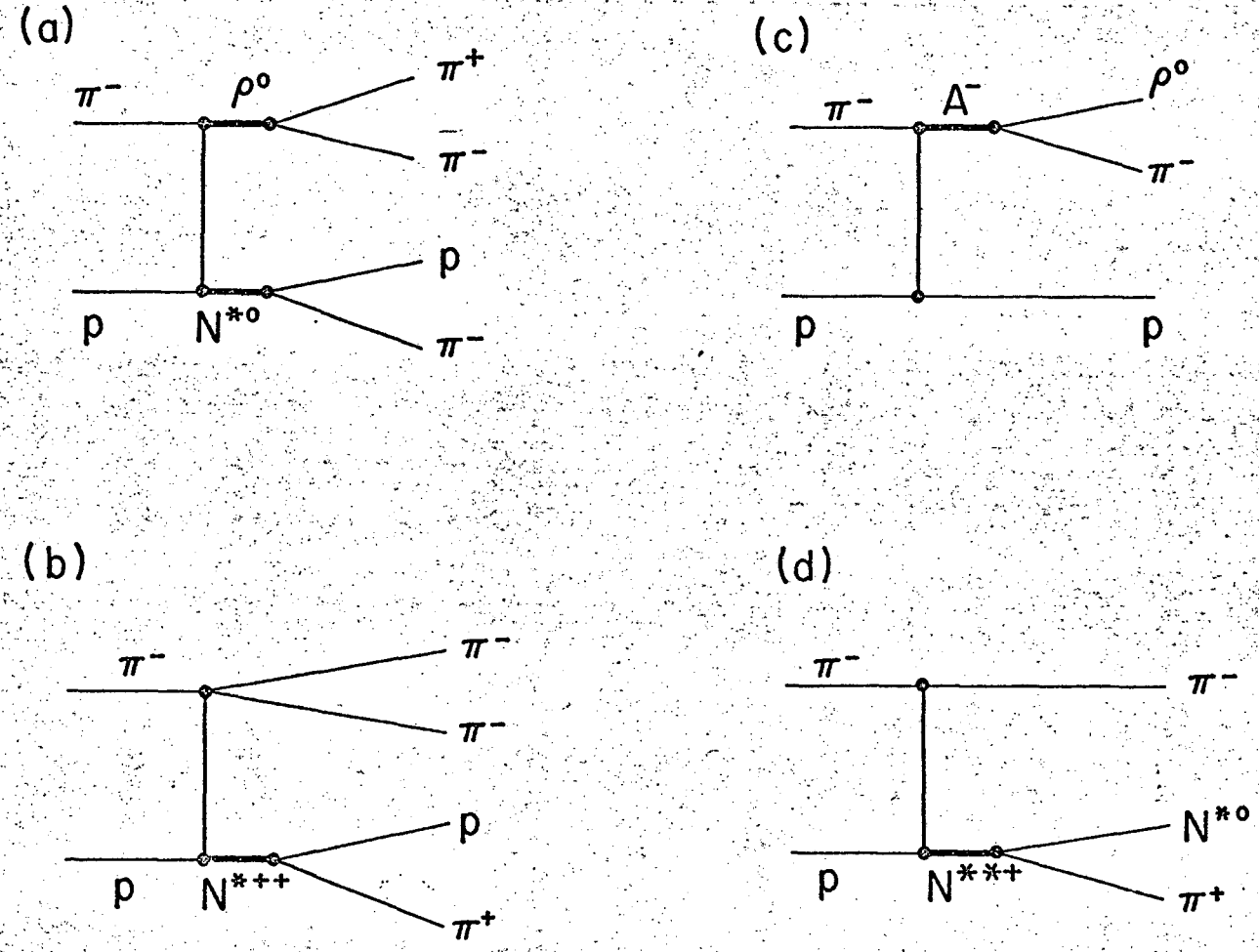

MUB-3421

Fig. 1

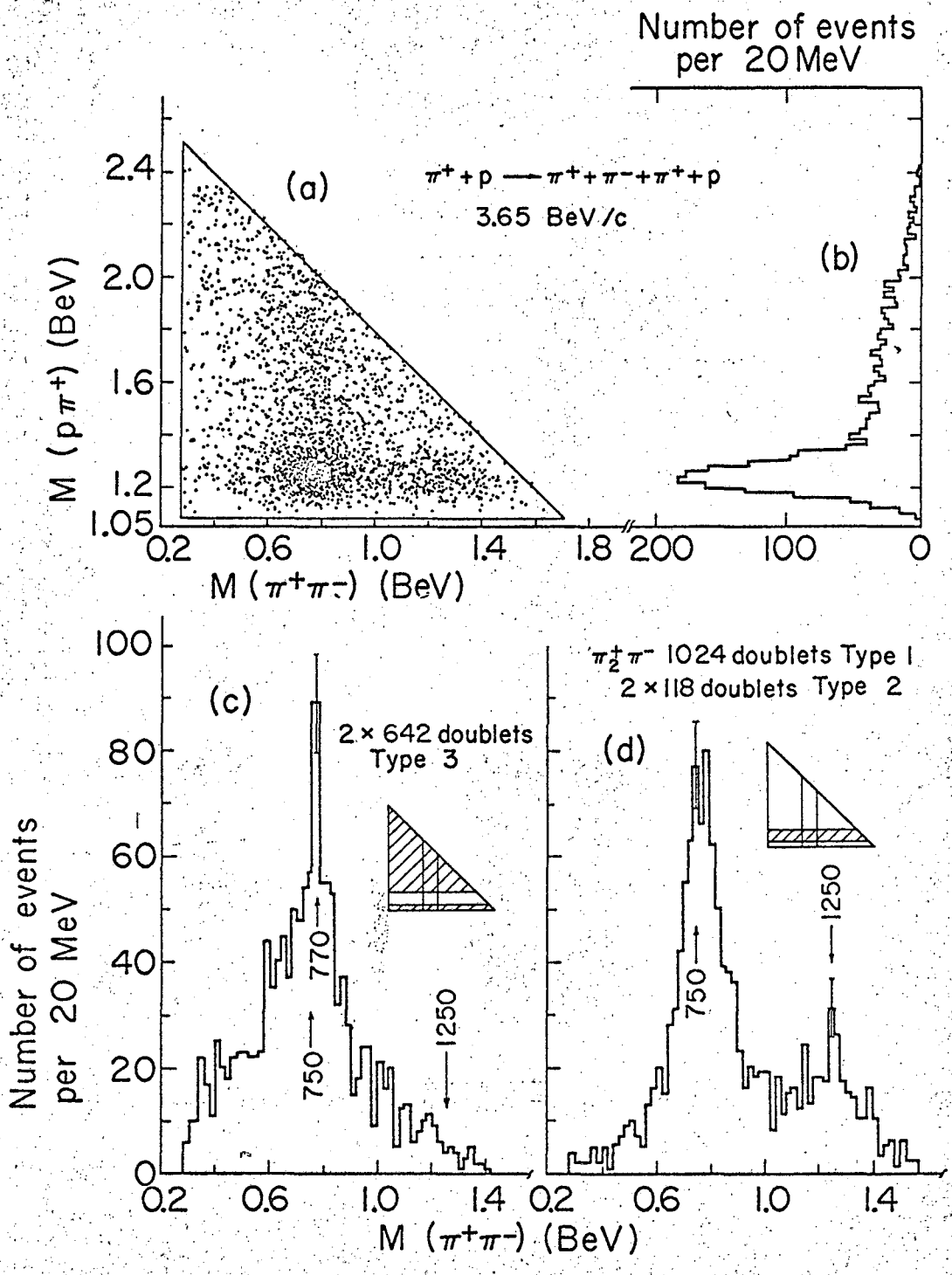
Number of events per 20 MeV
(a)
$\pi^+ + p \rightarrow \pi^+ + \pi^- + \pi^+ + p$
3.65 BeV/c
(b)
M ($p\pi^+$) (BeV)
2.4
2.0
1.6
1.2
1.05
0.2
0.6
1.0
1.4
1.8
200
100
0
M ($\pi^+\pi^-$) (BeV)
(c)
2 × 642 doublets Type 3
770
750
1250
$\pi_2^+\pi^-$ 1024 doublets Type 1
2 × 118 doublets Type 2
(d)
750
1250
Number of events per 20 MeV
100
80
60
40
20
0
0.2
0.6
1.0
1.4
M ($\pi^+\pi^-$) (BeV)

Fig. 2

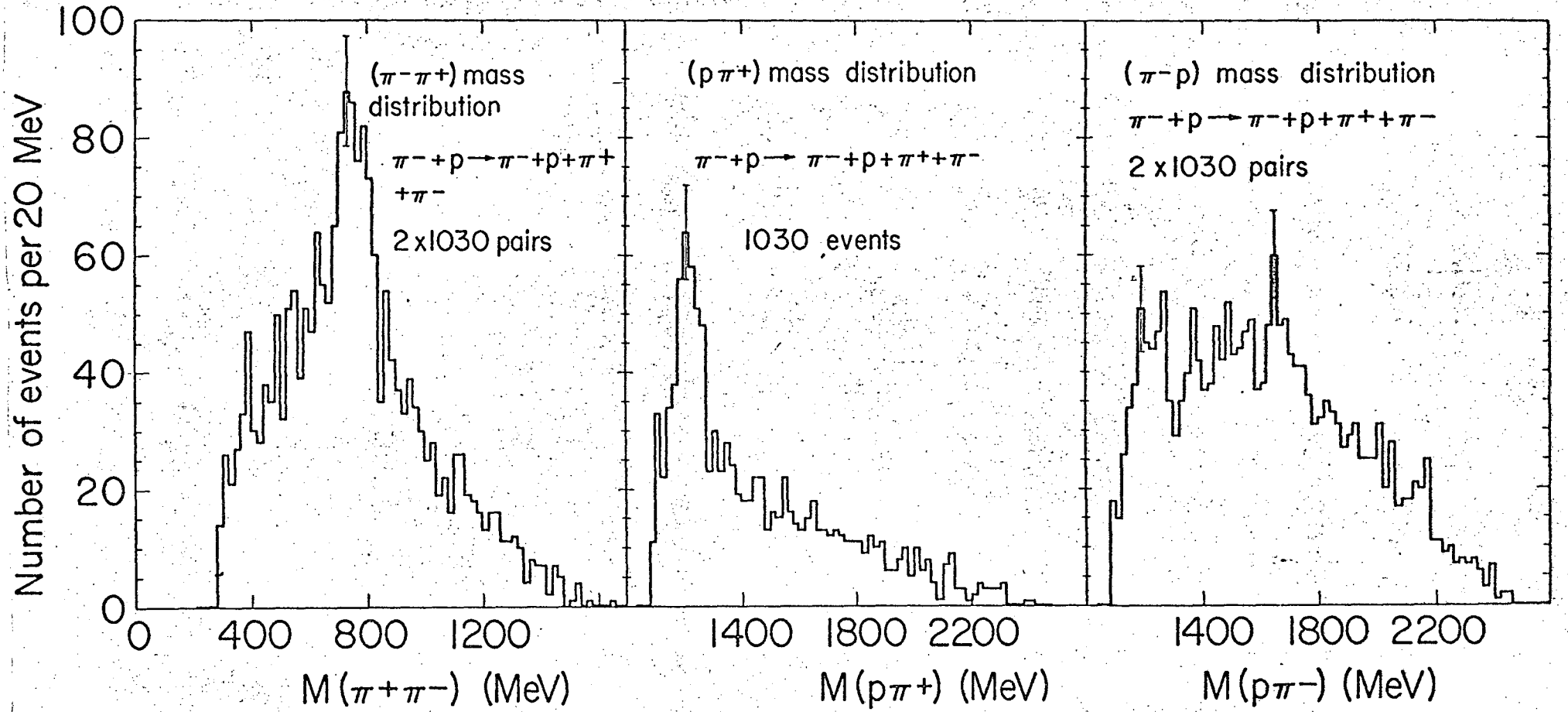

MUB-3429

Fig. 3

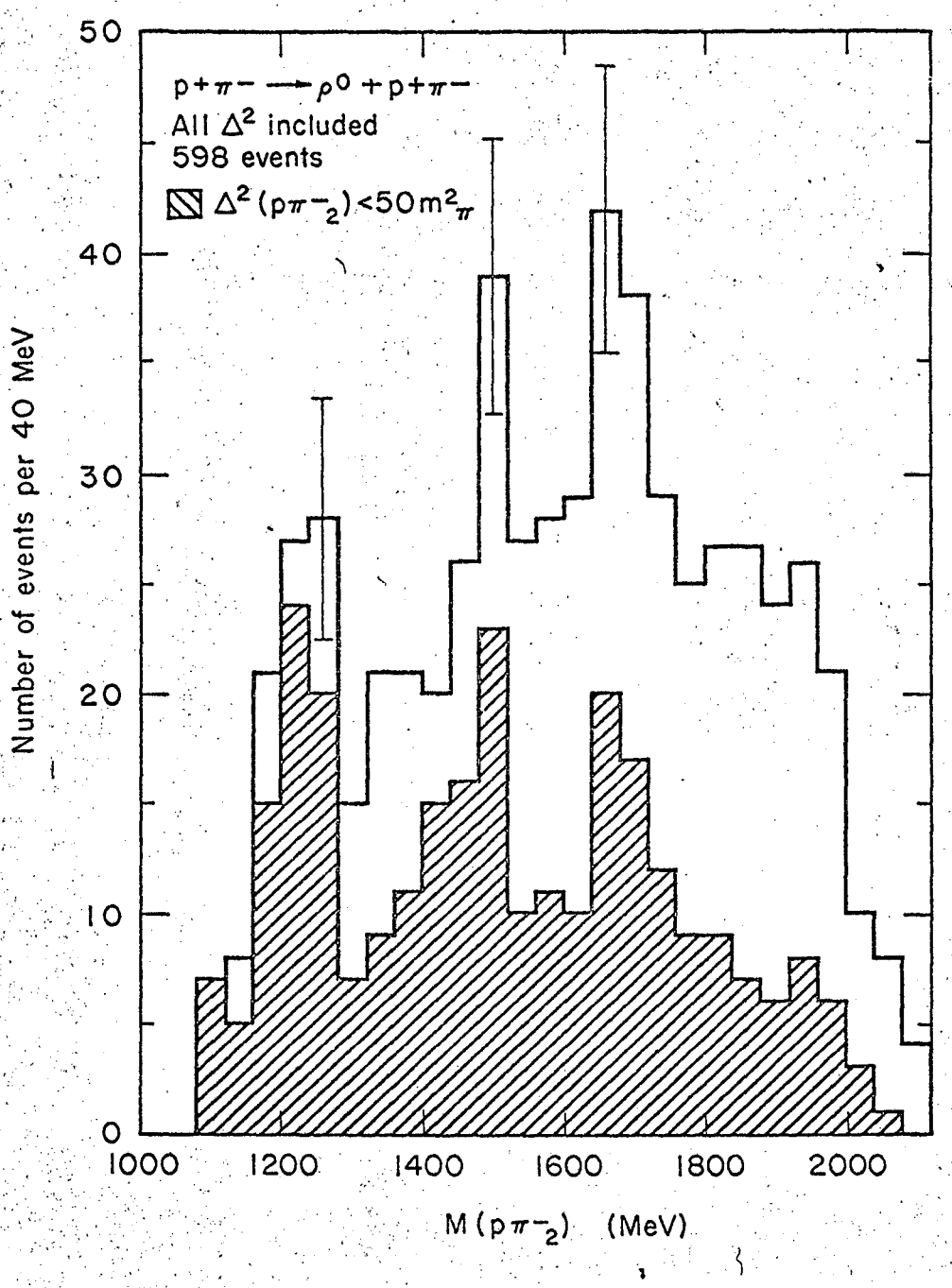
$p+\pi^- \longrightarrow \rho^0 + p+\pi^-$
All Δ^2 included
598 events
$\Delta^2(p\pi^-_2)<50 m^2_\pi$
Number of events per 40 MeV
0
10
20
30
40
50
1000
1200
1400
1600
1800
2000
$M(p\pi^-_2)$ (MeV)
MUB-3424

Fig. 4

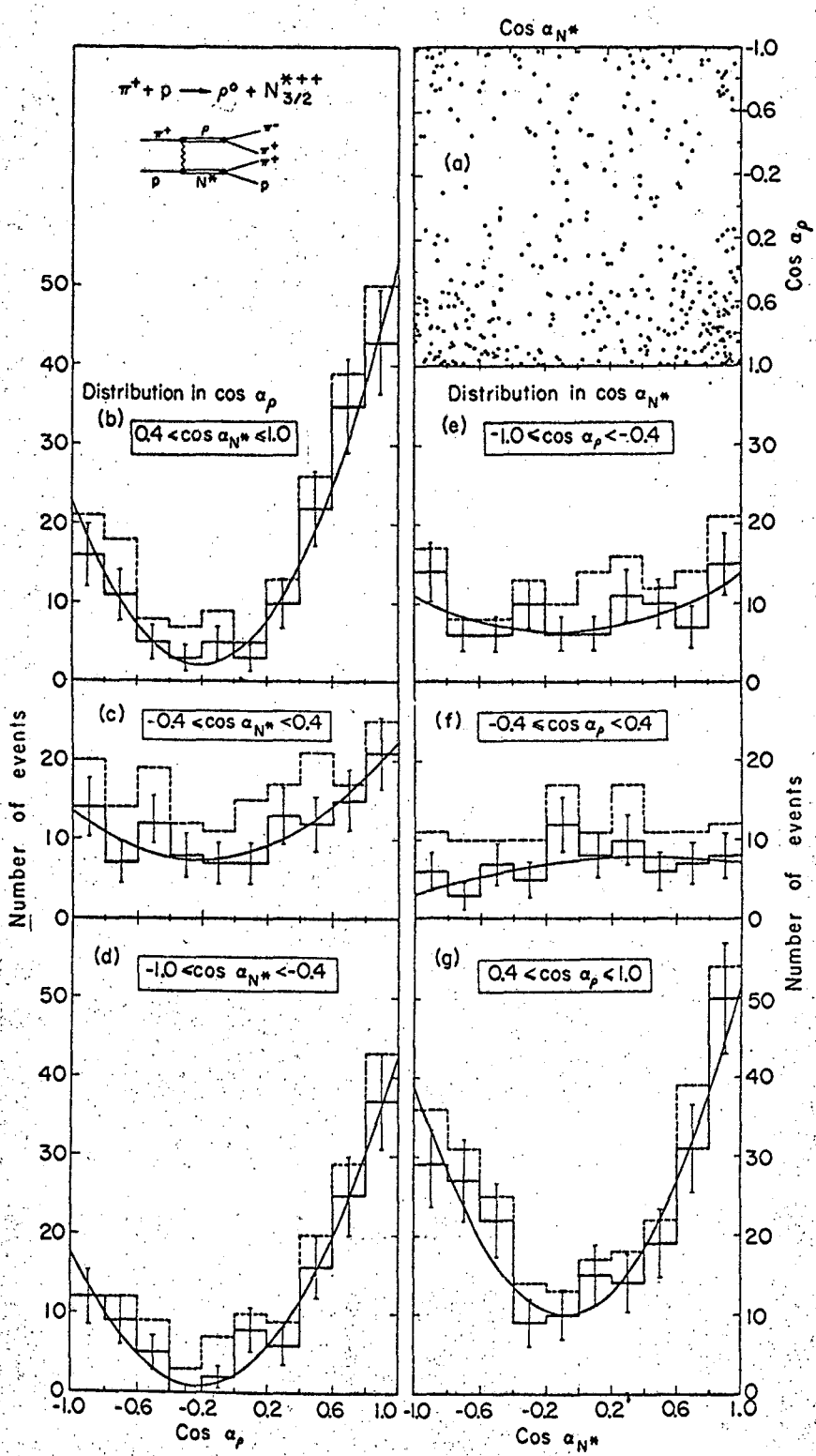
$\pi^+ + p \longrightarrow \rho^0 + N^{*++}_{3/2}$
Cos α_{N^*}
Cos α_ρ
(a)
Distribution in cos α_ρ
(b) 0.4 < cos α_{N^*} ≤ 1.0
Distribution in cos α_{N^*}
(e) -1.0 ≤ cos α_ρ < -0.4
(c) -0.4 < cos α_{N^*} < 0.4
(f) -0.4 ≤ cos α_ρ < 0.4
(d) -1.0 < cos α_{N^*} < -0.4
(g) 0.4 < cos α_ρ ≤ 1.0
Number of events
Cos α_ρ
Cos α_{N^*}

Fig. 5

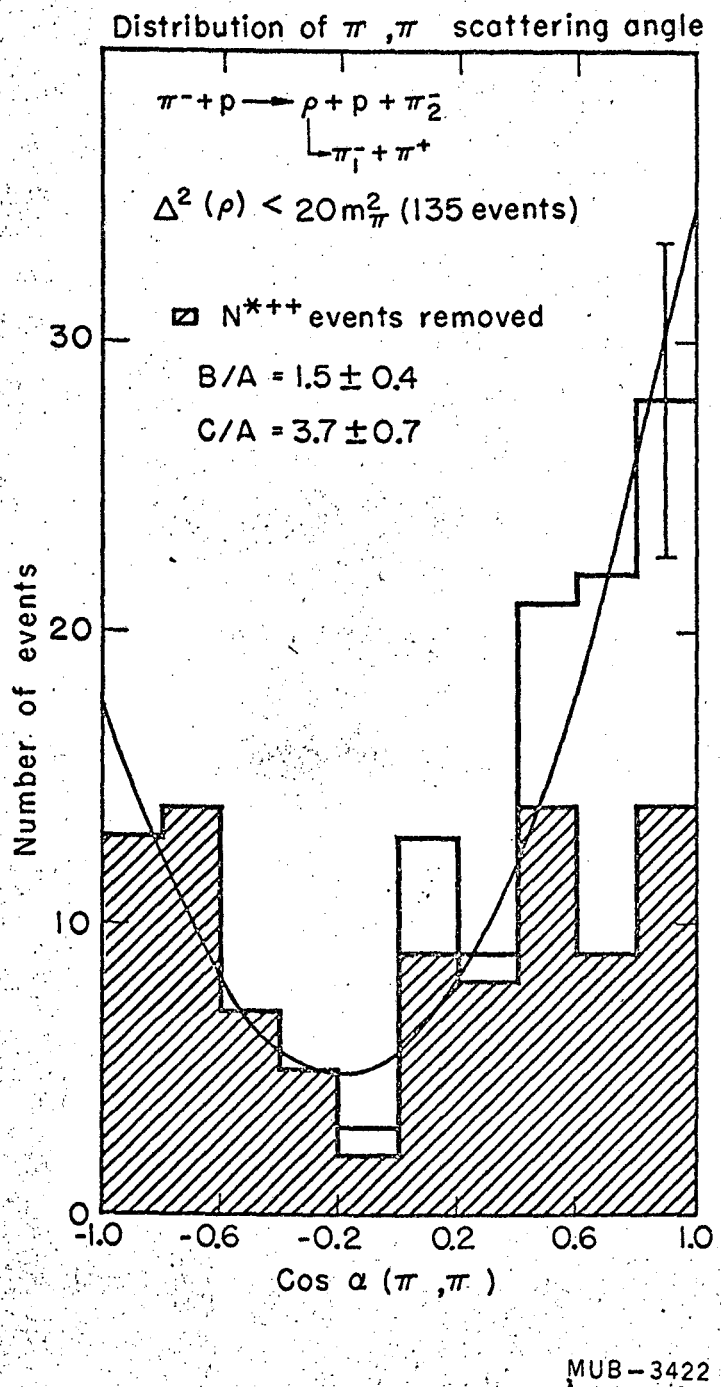
Distribution of π^-, π^- scattering angle
$\pi^- + p \rightarrow \rho + p + \pi_2^-$
$\rho \rightarrow \pi_1^- + \pi^+$
$\Delta^2(\rho) < 20 m_\pi^2$ (135 events)
N^{*++} events removed
B/A = 1.5 ± 0.4
C/A = 3.7 ± 0.7
Number of events
0
10
20
30
-1.0
-0.6
-0.2
0.2
0.6
1.0
Cos α (π^-, π^-)
MUB-3422

Fig. 6

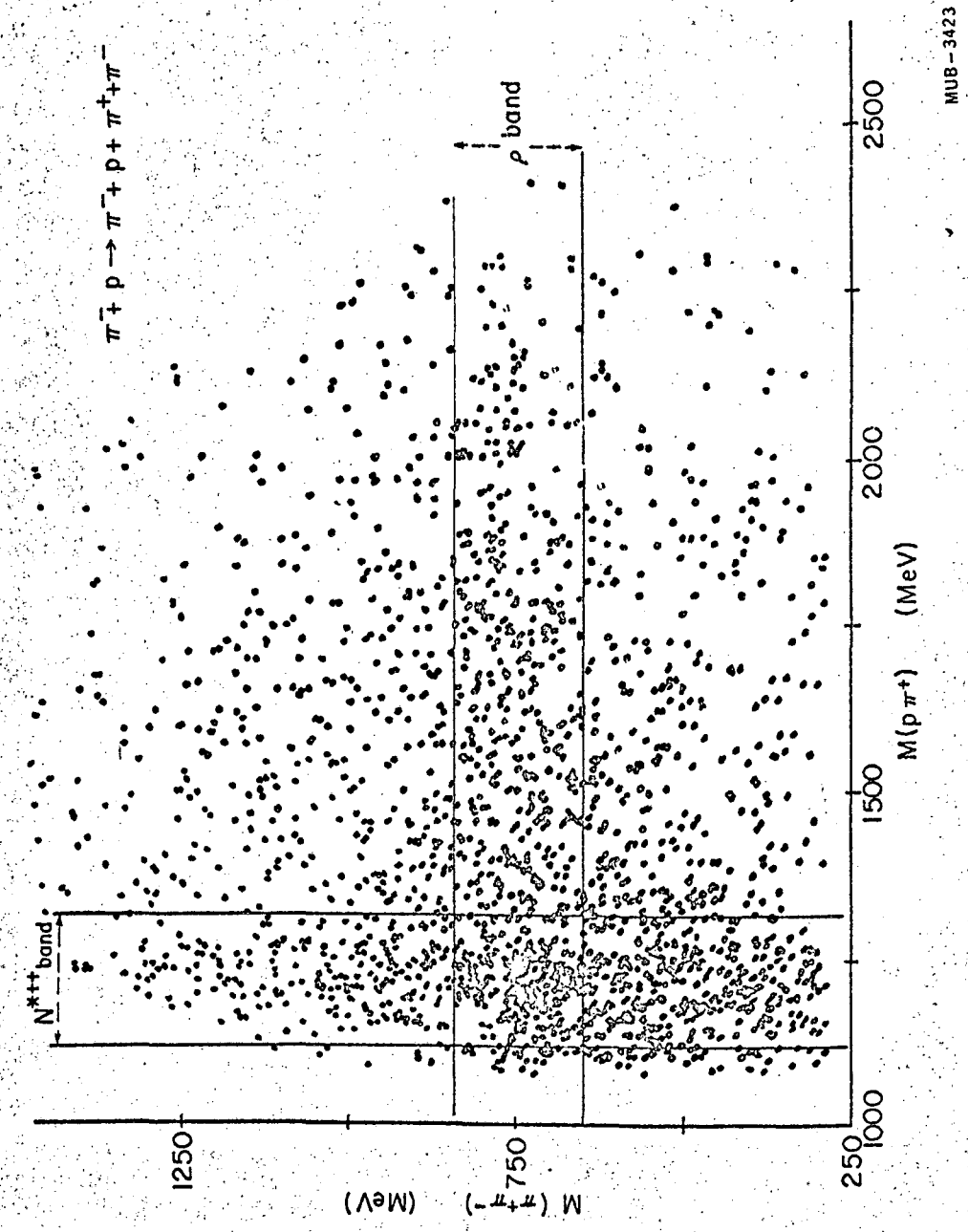
$\pi^- + p \rightarrow \pi^- + p + \pi^+ + \pi^-$
N^{*++} band
ρ band
M ($\pi^+\pi^-$) (MeV)
M($p\pi^+$) (MeV)
1250
750
250
1000
1500
2000
2500
MUB-3423

Fig. 7

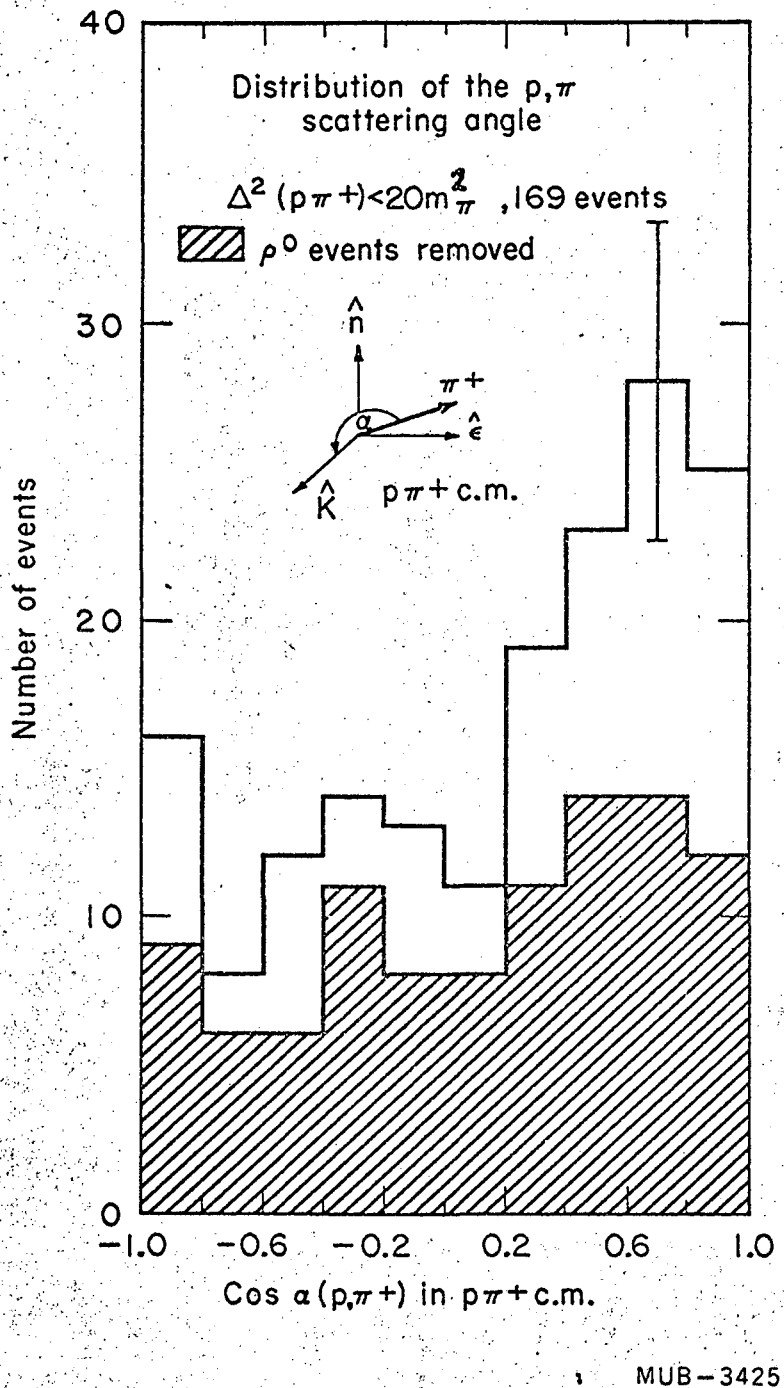
Distribution of the p,π scattering angle
Δ² (pπ+)<20m²π ,169 events
ρ⁰ events removed
n̂
π+
α
ε̂
K̂
pπ+ c.m.
Number of events
40
30
20
10
0
-1.0
-0.6
-0.2
0.2
0.6
1.0
Cos α (p,π+) in pπ+ c.m.
MUB-3425

Fig. 8

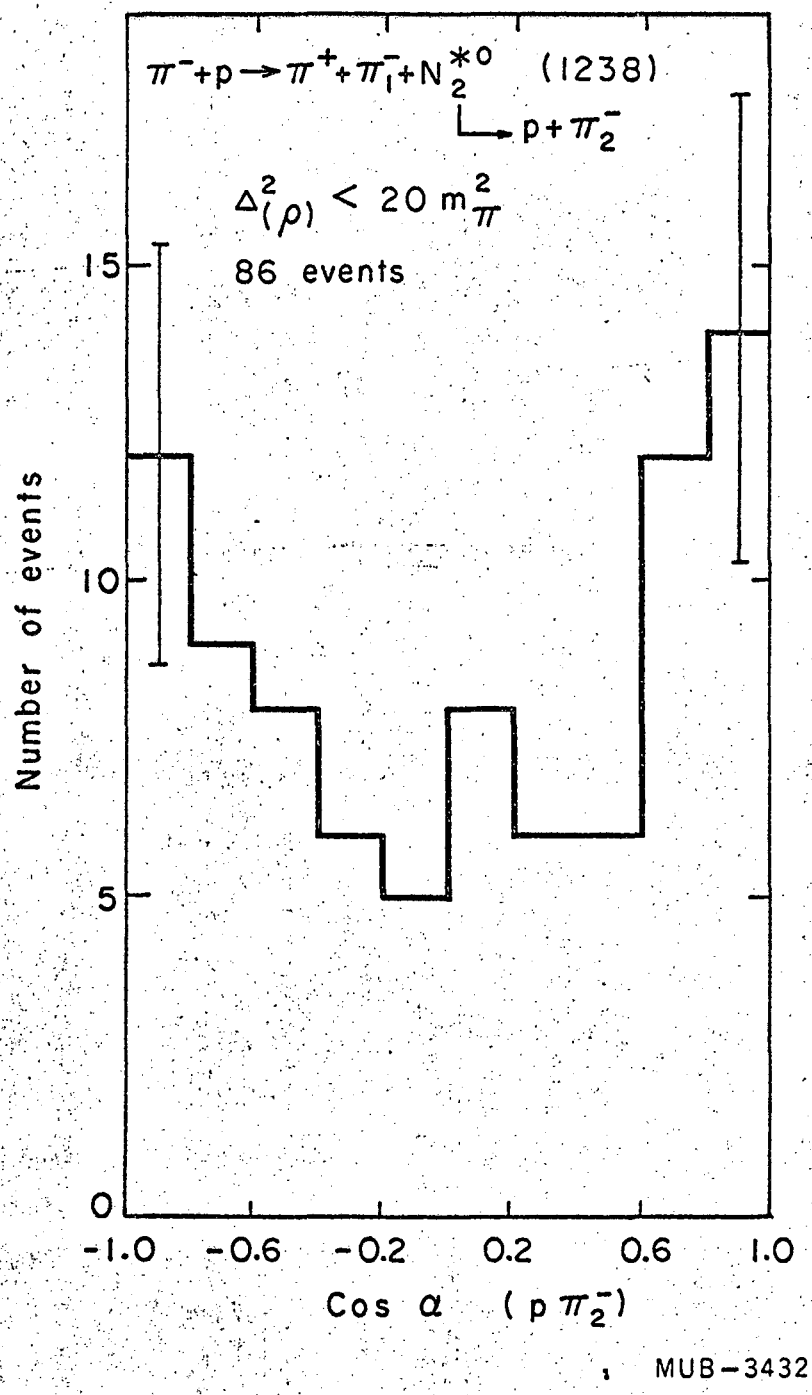
$\pi^- + p \rightarrow \pi^+ + \pi_1^- + N_2^{*0}$ (1238)
$\hookrightarrow p + \pi_2^-$
$\Delta^2_{(p)} < 20\, m^2_\pi$
86 events
Number of events
15
10
5
0
-1.0
-0.6
-0.2
0.2
0.6
1.0
Cos α ($p\pi_2^-$)
MUB-3432

Fig. 9

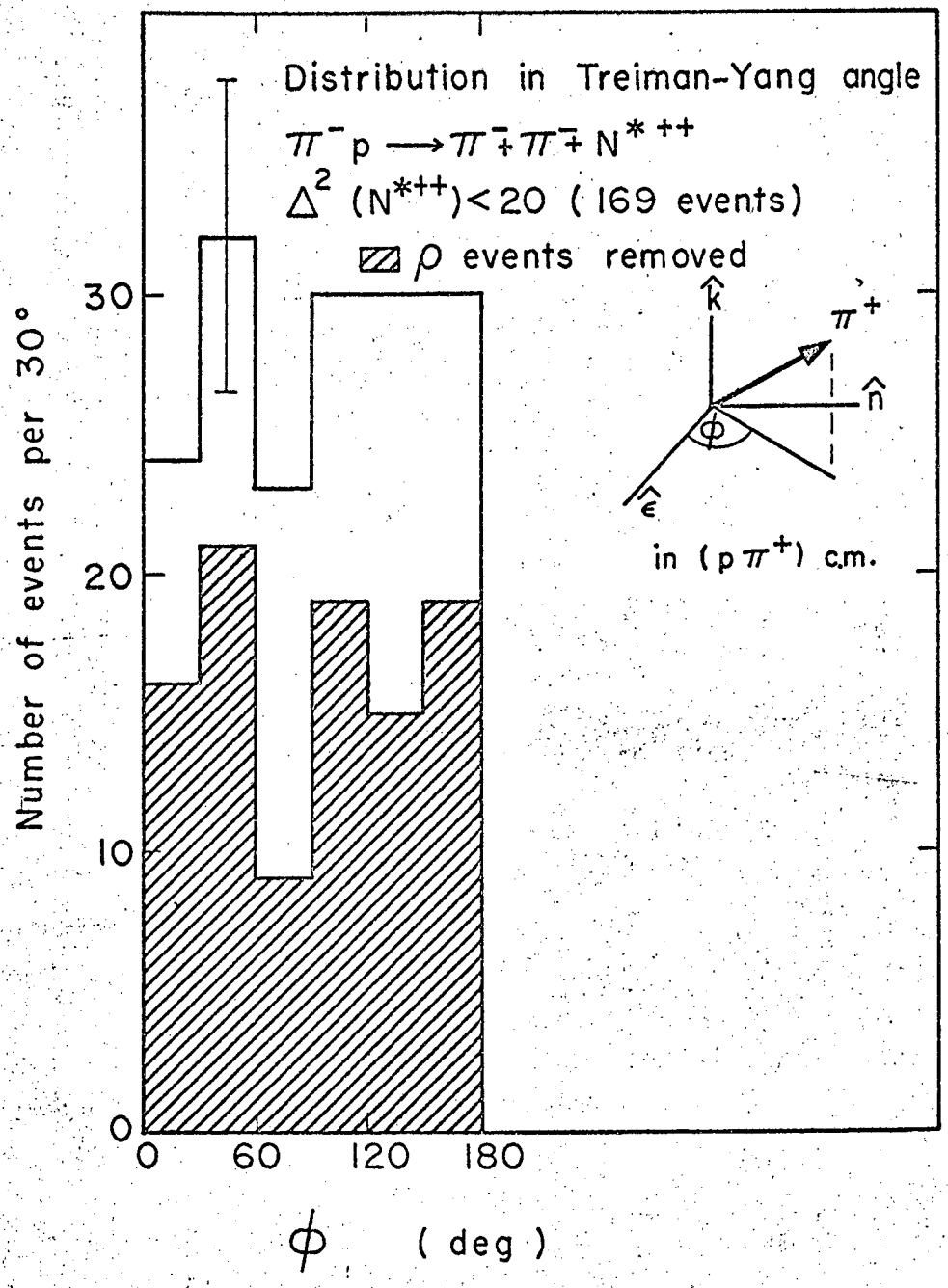

MUB-3427

Fig. 10

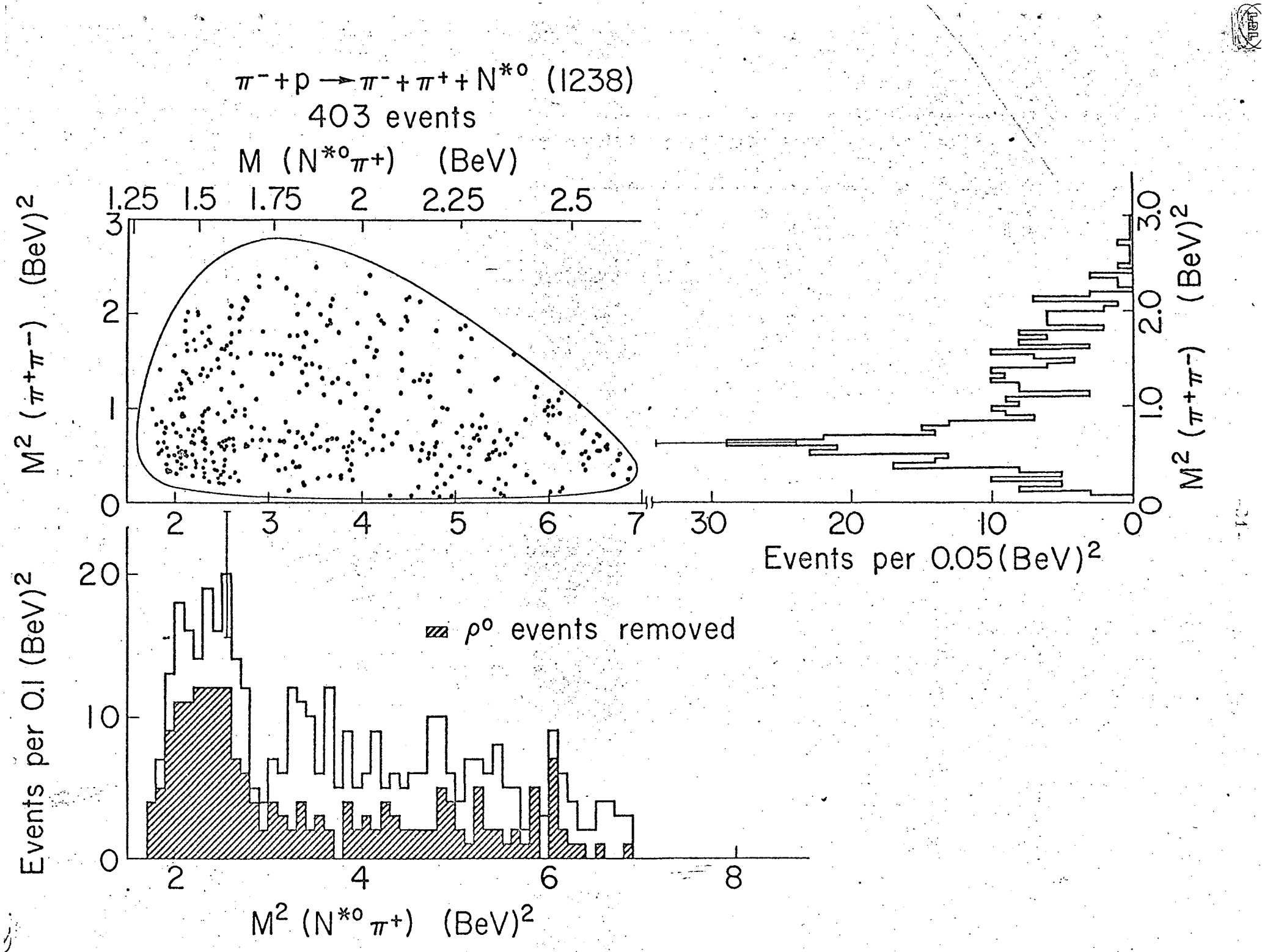
$\pi^- + p \rightarrow \pi^- + \pi^+ + N^{*0}$ (1238)
403 events
M ($N^{*0}\pi^+$) (BeV)
1.25 1.5 1.75 2 2.25 2.5
M^2 ($\pi^+\pi^-$) (BeV)^2
Events per 0.05(BeV)^2
Events per 0.1 (BeV)^2
ρ^0 events removed
M^2 ($N^{*0}\pi^+$) (BeV)^2

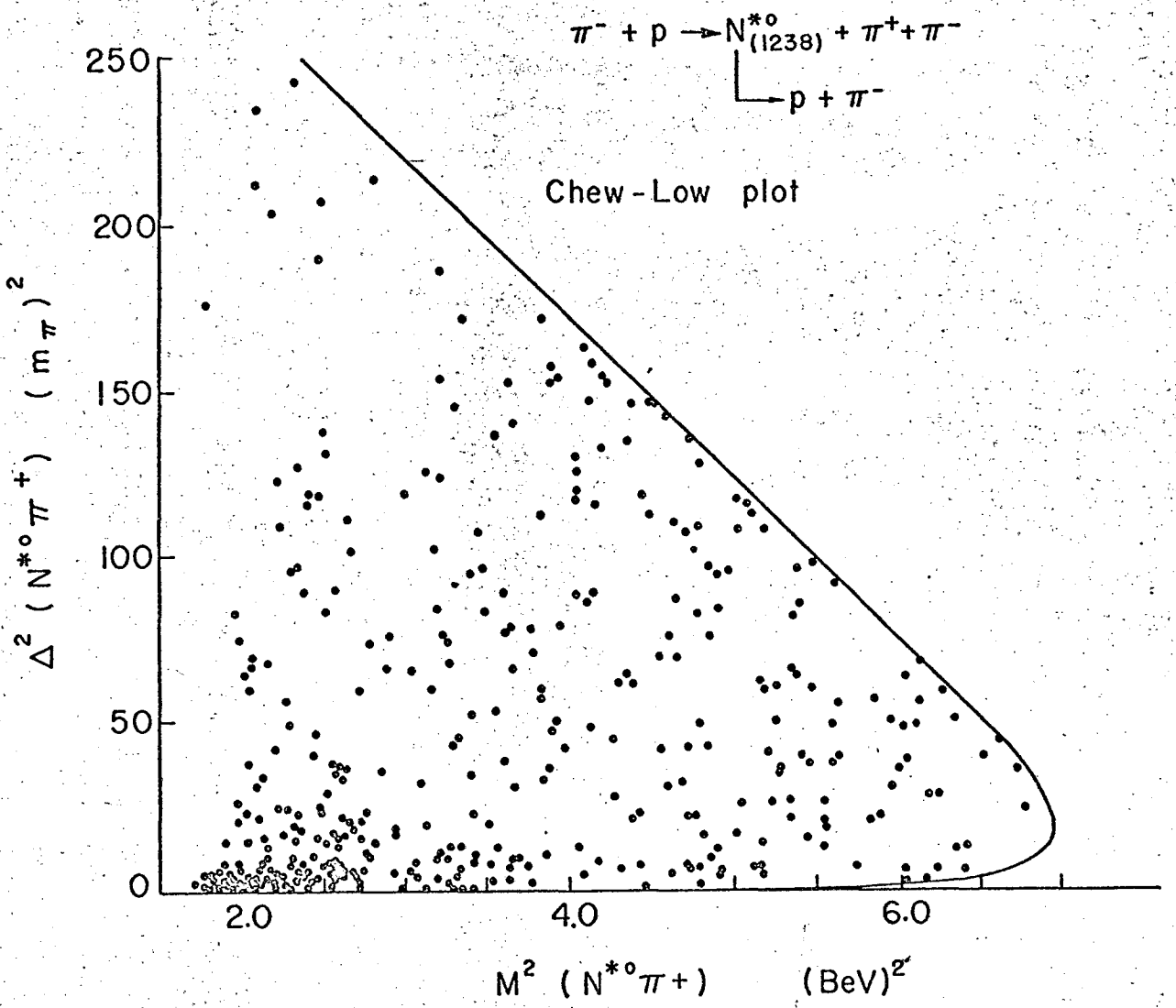
$\pi^- + p \rightarrow N^{*o}_{(1238)} + \pi^+ + \pi^-$
$\hookrightarrow p + \pi^-$
Chew-Low plot
250
200
150
100
50
0
2.0
4.0
6.0
$\Delta^2 (N^{*o}\pi^+)$ $(m_\pi)^2$
$M^2 (N^{*o}\pi+)$ $(BeV)^2$
MUB-3426

Fig. 12

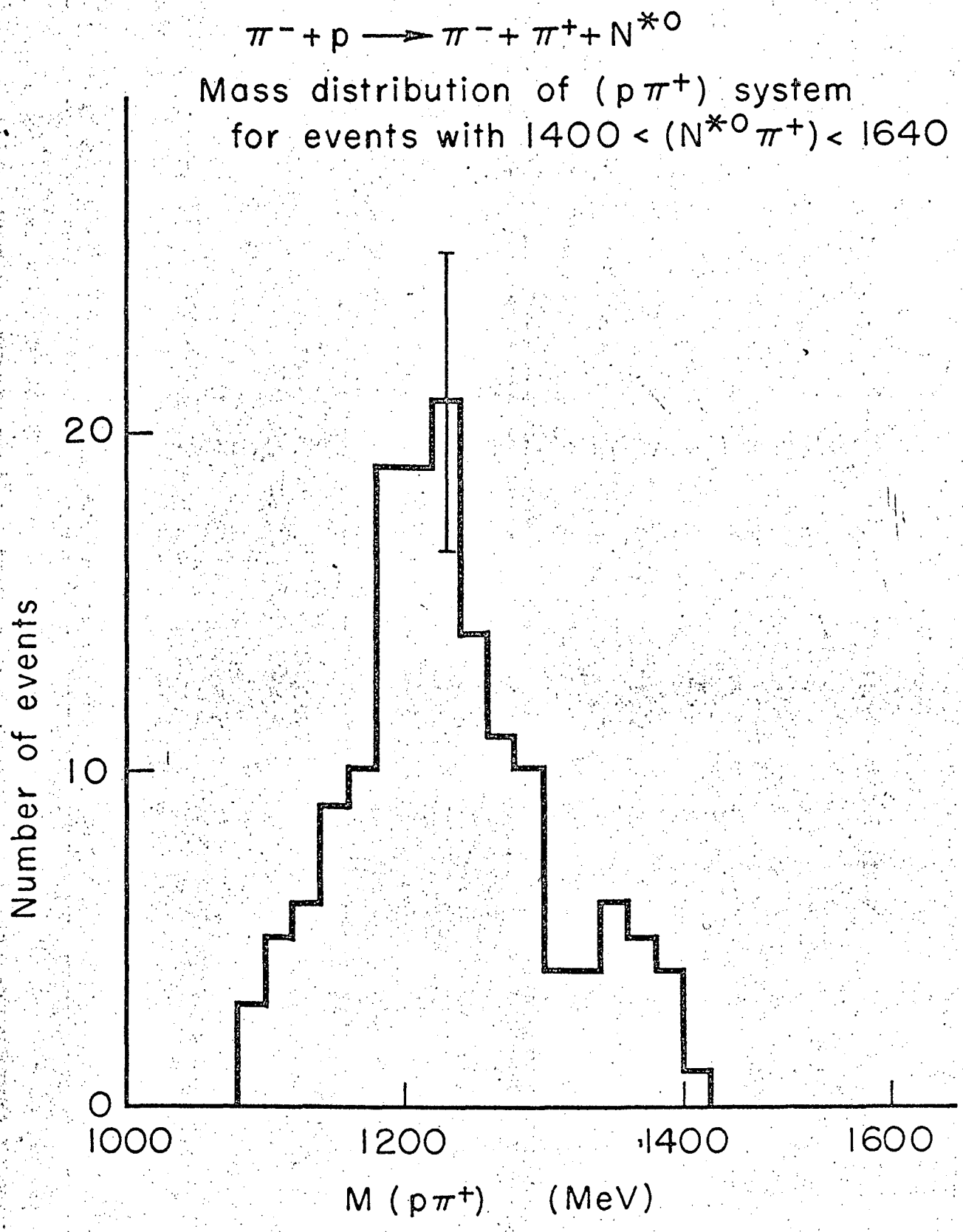
$\pi^- + p \longrightarrow \pi^- + \pi^+ + N^{*0}$
Mass distribution of $(p\pi^+)$ system
for events with $1400 < (N^{*0}\pi^+) < 1640$
Number of events
20
10
0
1000
1200
1400
1600
M $(p\pi^+)$ (MeV)

Fig. 13

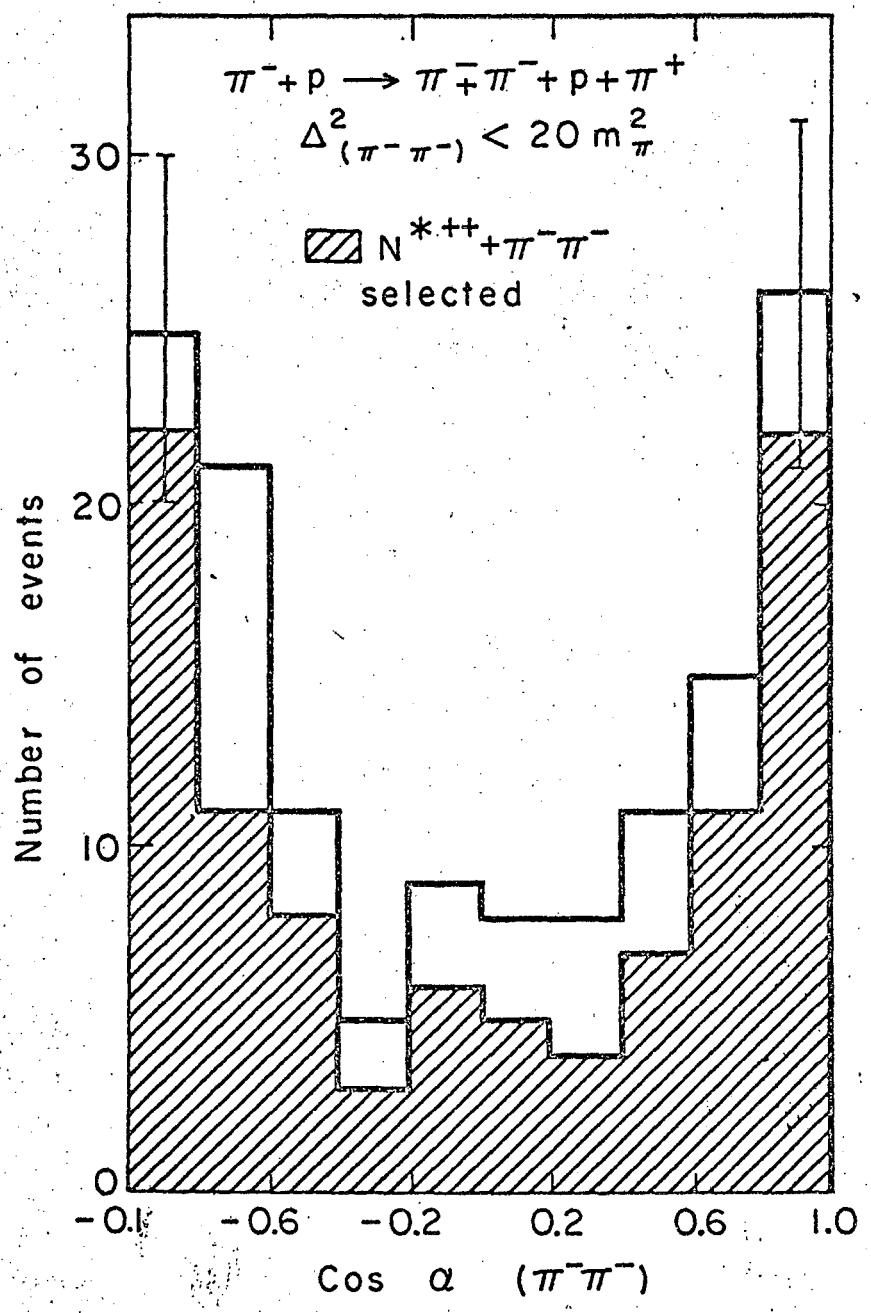
$\pi^- + p \longrightarrow \pi^{\mp}\pi^- + p + \pi^+$
$\Delta^2_{(\pi^-\pi^-)} < 20\, m^2_{\pi}$
$N^{*++} + \pi^-\pi^-$
selected
Number of events
30
20
10
0
-0.1
-0.6
-0.2
0.2
0.6
1.0
Cos α $(\pi^-\pi^-)$
MUB-3430

Fig. 14